12. Y. Hyakutake, *Prog. Theor. Exp. Phys.* **033B04**, 1–27 (2014).
13. J. Polchinski, *Phys. Rev. Lett.* **75**, 4724–4727 (1995).
14. E. Witten, *Nucl. Phys. B* **460**, 335–350 (1996).
15. N. Itzhaki, J. M. Maldacena, J. Sonnenschein, S. Yankielowicz, *Phys. Rev. D* **58**, 046004 (1998).
16. J. A. Minahan *et al.*, *Lett. Math. Phys.* **99**, 33–58 (2012).
17. Although we study dynamical aspects of the duality in the present work, certain kinematical aspects of the duality have been tested recently at the level of quantum gravity (*30*).
18. T. Banks, W. Fischler, S. H. Shenker, L. Susskind, *Phys. Rev. D* **55**, 5112–5128 (1997).
19. B. de Wit, J. Hoppe, H. Nicolai, *Nucl. Phys. B* **305**, 545–581 (1988).
20. Theoretical consistency requires that superstring theory should be defined in 10D space-time. To realize our 4D space-time, the size of the extra six dimensions can be very small without spoiling the consistency.
21. M. Hanada, J. Nishimura, S. Takeuchi, *Phys. Rev. Lett.* **99**, 161602 (2007).
22. K. N. Anagnostopoulos, M. Hanada, J. Nishimura, S. Takeuchi, *Phys. Rev. Lett.* **100**, 021601 (2008).
23. M. Hanada, Y. Hyakutake, J. Nishimura, S. Takeuchi, *Phys. Rev. Lett.* **102**, 191602 (2009).
24. M. Hanada, J. Nishimura, Y. Sekino, T. Yoneya, *J. High Energy Phys.* **1112**, 020 (2011).
25. D. Kabat, G. Lifschytz, D. A. Lowe, *Phys. Rev. Lett.* **86**, 1426–1429 (2001).
26. S. Catterall, T. Wiseman, *Phys. Rev. D* **78**, 041502 (2008).
27. Materials and methods are available as supplementary materials on *Science* Online.
28. S. Dürr *et al.*, *Science* **322**, 1224–1227 (2008).
29. N. Ishii, S. Aoki, T. Hatsuda, *Phys. Rev. Lett.* **99**, 022001 (2007).
30. A. Arabi Ardehali, J. T. Liu, P. Szepietowski, *J. High Energy Phys.* **1306**, 024 (2013).

ACKNOWLEDGMENTS

The authors would like to thank S. Aoki, S. Hartnoll, I. Kanamori, H. Kawai, E. Poppitz, A. Schäfer, S. Shenker, L. Susskind, M. Tezuka, A. Ueda, and M. Ünsal for discussions and comments. M.H. is supported by the Hakubi Center for Advanced Research, Kyoto University and by the National Science Foundation under grant no. PHYS-1066293. M.H. and Y.H. are partially supported by the Ministry of Education, Science, Sports and Culture, Grant-in-Aid for Young Scientists (B), 25800163, 2013 (M.H.); 19740141, 2007 (Y.H.); and 24740140, 2012 (Y.H.). The work of J.N. was supported in part by Grant-in-Aid for Scientific Research (nos. 20540286 and 23244057) from the Japan Society for the Promotion of Science. Computations were carried out on PC cluster systems in KEK and the Osaka University Cybermedia Center (the latter being provided by the High Performance Computing Infrastructure System Research Project, project ID: hp120162). All the data obtained in the present work are presented in table S1 of the supplementary materials.

SUPPLEMENTARY MATERIALS

www.sciencemag.org/content/344/6186/882/suppl/DC1
Materials and Methods
Supplementary Text
Fig. S1
Table S1
References (*31*–*35*)

23 December 2013; accepted 31 March 2014
Published online 17 April 2014;
10.1126/science.1250122

CHEMISTRY

Real-space imaging of molecular structure and chemical bonding by single-molecule inelastic tunneling probe

Chi-lun Chiang,[1]* Chen Xu,[1]* Zhumin Han,[1]* W. Ho[1,2]†

The arrangement of atoms and bonds in a molecule influences its physical and chemical properties. The scanning tunneling microscope can provide electronic and vibrational signatures of single molecules. However, these signatures do not relate simply to the molecular structure and bonding. We constructed an inelastic tunneling probe based on the scanning tunneling microscope to sense the local potential energy landscape of an adsorbed molecule with a carbon monoxide (CO)–terminated tip. The skeletal structure and bonding of the molecule are revealed from imaging the spatial variations of a CO vibration as the CO-terminated tip probes the core of the interactions between adjacent atoms. An application of the inelastic tunneling probe reveals the sharing of hydrogen atoms among multiple centers in intramolecular and extramolecular bonding.

The achievement of a mechanistic understanding of chemical and biological functions depends on knowing the geometric structure and the nature of the bonds in the molecules. Consequently, a number of techniques have been extensively developed to attain this knowledge, including x-ray diffraction, electron diffraction, and nuclear magnetic resonance. These techniques, however, do not provide a direct view of the molecules in real space. Nonetheless, they have yielded three-dimensional structures of many complex molecules that enabled the elucidation of their chemical and biological properties. Only recently has the atomic force microscope (AFM) been used to obtain real-space images of the molecular structures of mostly planar molecules (*1*, *2*). The AFM approach allows structural imaging that can discriminate a reactant and its different products (*3*) or reveal hydrogen bonding between molecules (*4*).

The high spatial resolution of the AFM was obtained by functionalizing the tip with a CO molecule (*5*, *6*) and measuring the shift in the resonance frequency of the quartz tuning fork above the adsorbed molecule (*7*). The spatial resolution arises from variations of the force gradient sensed by the CO-tip as it scans over different parts of the molecule. The observed contrast revealing the molecular structure implies that the frequency shift is different over the atoms and the bonds between them, relative to elsewhere. The range of frequency shift is few Hz from the resonance of 20 to 30 kHz.

In comparison, the scanning tunneling microscope (STM) has been shown to reveal the electronic properties of the sample. Good agreements have been obtained between theory and experiment for the molecular orbitals in describing the spatial distributions for the electron density (*8*–*10*) and spin excitation (*11*). These images reflect the electron wave functions that are related to (but do not directly display) the molecular structures. By trapping a hydrogen molecule in the STM junction or transferring a Xe, CO, or CH_4 molecule to the tip, molecular structure could be resolved from the topographic and differential conductance images, and intermolecular bonds were revealed (*12*–*14*).

Here, we demonstrate an approach based on the STM to image the skeletal structure and bonding in an adsorbed molecule by single-molecule inelastic tunneling probe (itProbe). A CO molecule is transferred to the tip, and a vibrational mode of the tip CO senses the bonding between two atoms in an adsorbed molecule. As the CO-terminated tip is scanned over the molecule during imaging, changes in the energy and intensity of the hindered translational vibration of CO are measured by inelastic electron tunneling spectroscopy (IETS) with the STM (*15*). This low-energy CO vibration senses the spatially varying potential energy landscape of the molecule and its surroundings. The range of energy shift is on the order of the vibrational energy of ~3 meV, or equivalently ~0.7 THz.

All of the experiments were performed in ultrahigh vacuum (5×10^{-11} torr); the spectra reported were taken at a sample and STM temperature of 600 mK (*16*). A topographic image taken with a bare Ag tip of cobalt phthalocyanine (CoPc) coadsorbed with CO on Ag(110) is shown in Fig. 1A. Adsorption configurations, labeled CoPc(×) and CoPc(+), are possible on the surface. Each CO molecule is identified by its hindered translational (2.8 meV) and rotational (18.3 and 20.3 meV) modes in the vibrational spectra by STM-IETS (Fig. 1B). The nondegenerate hindered rotation in the two orthogonal directions parallel to the Ag(110) surface is resolved as a peak splitting. The same area imaged after

[1]Department of Physics and Astronomy, University of California, Irvine, CA 92697, USA. [2]Department of Chemistry, University of California, Irvine, CA 92697, USA.
*These authors contributed equally to this work. †Corresponding author. E-mail: wilsonho@uci.edu

transferring a CO molecule (marked by arrow in Fig. 1A) to the tip is shown in Fig. 1C. The presence of CO on the tip is confirmed by STM-IETS taken at any location over the clean Ag surface (Fig. 1D). The energies of the hindered translational (2.1 meV) and rotational (18.2 meV) modes are close to those of CO on the Ag surface as recorded by the bare tip.

Vibrational spectra can be recorded by STM-IETS with high spatial resolution at a chosen position (point spectroscopy) over an adsorbed molecule (*15*, *17*) and with bare, CO-terminated, and ethylene-terminated tips (*18*). In the scanned energy range, vibrational modes are resolved for CO but not for CoPc. As the CO-terminated tip

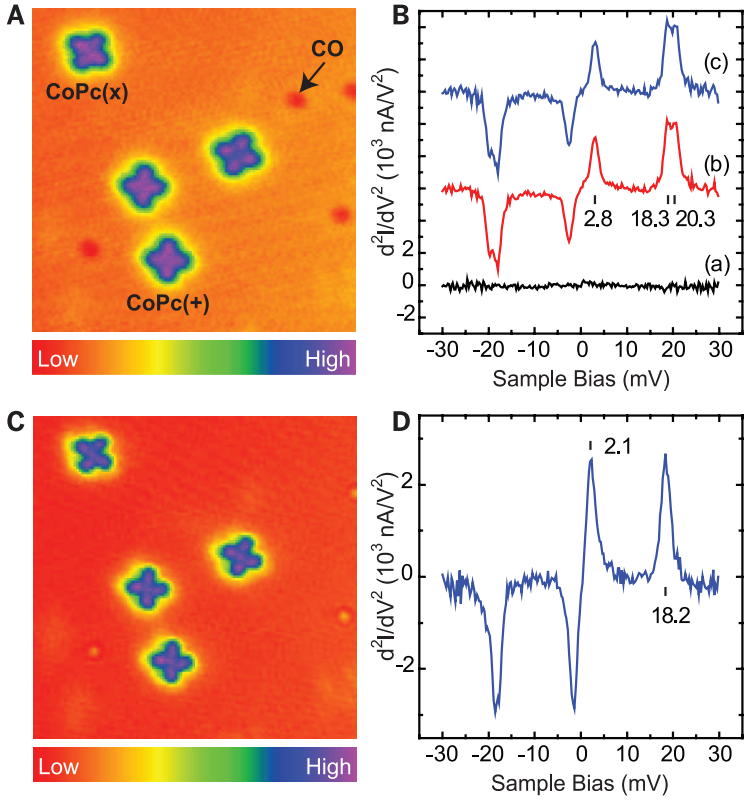

Fig. 1. The creation and characterization of a CO-terminated tip. (**A**) Constant-current topography of CO coadsorbed with CoPc(×) and CoPc(+) on Ag(110) at 600 mK (121.1 Å × 121.1 Å). Tunneling gap set point: V = 0.1 V and I = 0.1 nA. (**B**) Vibrational STM-IETS d^2I/dV^2 spectra taken with a bare tip over the Ag surface (a), CO molecule (b), and the background-subtracted spectrum (c). Bias root mean square (RMS) voltage modulation: 0.6 mV at 471 Hz. Set point: V = 10.0 mV and I = 1.0 nA. (**C**) Constant-current topography of the same area as in (A) after transferring a CO [the one indicated by the arrow in (A)] to the tip. CO is imaged as a protrusion instead of a depression. (**D**) Vibrational STM-IETS d^2I/dV^2 spectrum of CO-terminated tip taken over the Ag surface. Bias RMS voltage modulation: 0.6 mV at 471 Hz. Set point: V = 10.0 mV and I = 1.0 nA.

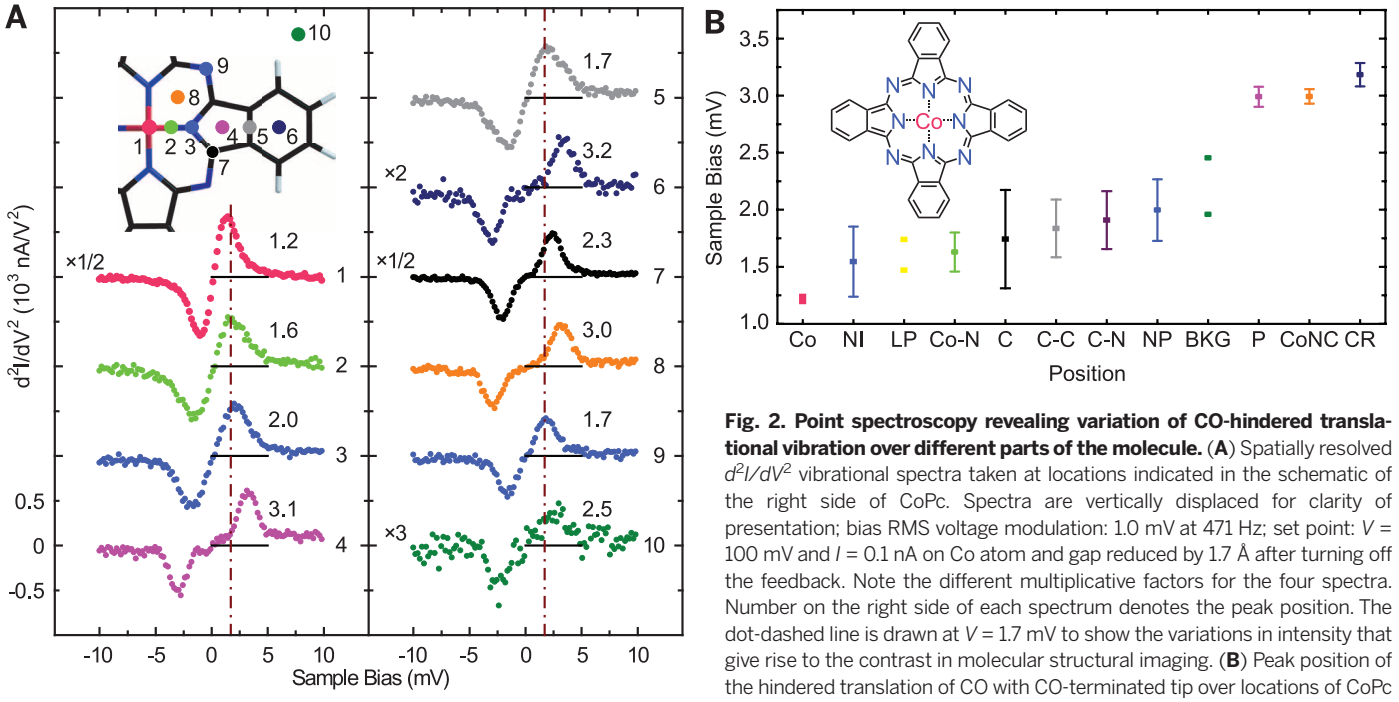

Fig. 2. Point spectroscopy revealing variation of CO-hindered translational vibration over different parts of the molecule. (**A**) Spatially resolved d^2I/dV^2 vibrational spectra taken at locations indicated in the schematic of the right side of CoPc. Spectra are vertically displaced for clarity of presentation; bias RMS voltage modulation: 1.0 mV at 471 Hz; set point: V = 100 mV and I = 0.1 nA on Co atom and gap reduced by 1.7 Å after turning off the feedback. Note the different multiplicative factors for the four spectra. Number on the right side of each spectrum denotes the peak position. The dot-dashed line is drawn at V = 1.7 mV to show the variations in intensity that give rise to the contrast in molecular structural imaging. (**B**) Peak position of the hindered translation of CO with CO-terminated tip over locations of CoPc molecule indicated on the x axis: Co (cobalt atom), NI (imine nitrogen), LP (lone pair on imine nitrogen), Co-N (cobalt-pyrrole nitrogen bond), C (carbon atom), C-C bond, C-N bond, NP (pyrrole nitrogen), BKG (Ag substrate), P (pyrrole ring), CoNC (CoNCNCN ring), CR (six-member carbon ring). Inset shows a schematic diagram of CoPc. There are only two data points for Co, LP, and BKG, hence no error bars.

is scanned over the CoPc, the percent change in the vibrational energy is larger for the hindered translation relative to the hindered rotation. Furthermore, the noise in the current decreases as the bias voltage is lowered. Both factors favor the hindered translational vibration for sensing the CoPc.

The sensitivity of the hindered translational mode of CO to its position over a CoPc molecule is shown by vibrational point spectroscopy in Fig. 2A. A clear vibrational energy upshift by ~2.0 meV is measured as the spectrum is recorded over the central Co atom (point 1; 1.2 meV) instead of over the center of the five-member pyrrole ring (point 4; 3.1 meV), the six-member carbon ring (point 6; 3.2 meV), and the inner six-member CoNC ring (point 8; 3.0 meV). The vibrational energy is <2.5 meV for spectra taken over other points of the molecule. The intensity over the Ag background is weaker than over the molecule. Figure 2A shows the spectra taken over 10 selected points of the molecule and the Ag background (a more comprehensive set of spectra is given in fig. S1; 57 locations over the molecule are labeled in fig. S2E). The bias voltage at the peak of each spectrum in fig. S1 is plotted in Fig. 2B; the error bars show the spread in the peak energy centered over the average value. Possible sources for this spread include (i) incommensurability between molecule and substrate, (ii) atomic unevenness of molecule and substrate, (iii) spatial variation in the tip-CO tilt, and (iv) imprecise positioning of the tip over the molecule.

The CO-terminated tip can be used for energy-resolved spatial imaging of the molecule. When the energy is chosen within the CO-hindered translational vibration and <2.5 meV, the image reveals the skeletal structure of CoPc using either the constant-height or constant-current mode (*16*), as shown in Fig. 3, A and B, for CoPc(+). A structural image for CoPc(×) is shown in Fig. 3C; the arrows point to the four lone pairs of the imine nitrogen, each forming intramolecular hydrogen bonds with the two nearest C-H bonds. The CoPc(+) in Fig. 3B is shown schematically in Fig. 3D; the dashed lines indicate the intramolecular hydrogen bonds. Such bonding has been tentatively discussed in structural images taken with the AFM (*19*). In contrast, these intramolecular hydrogen bonds appear to be absent when the CoPc is adsorbed on the Au(110)2×1 reconstructed surface (Fig. 3E) where every other row of Au atoms is missing. The C-H bonds of CoPc on the Au(110)2×1 project outward, as shown by dashed lines in Fig. 3F. The schematic of CoPc is superimposed and compared to the structural images in fig. S3. The molecular structure and bonds are imaged with different resolutions using constant-height versus constant-current modes, as shown in Fig. 3 and further supported in figs. S4 and S5. Evidently, images of the skeletal structure and spectroscopic sensitivity to different atoms, bonds, and regions in the molecule are achieved by the itProbe. Bonds, rather than densities of states and molecular orbitals, are imaged by itProbe and reflect localized interactions or bonds between adjacent atoms.

Some C-H bonds of CoPc on the Au(110)2×1 surface are imaged as "V" shapes in Fig. 3E and marked in Fig. 3F, exhibiting bifurcation of

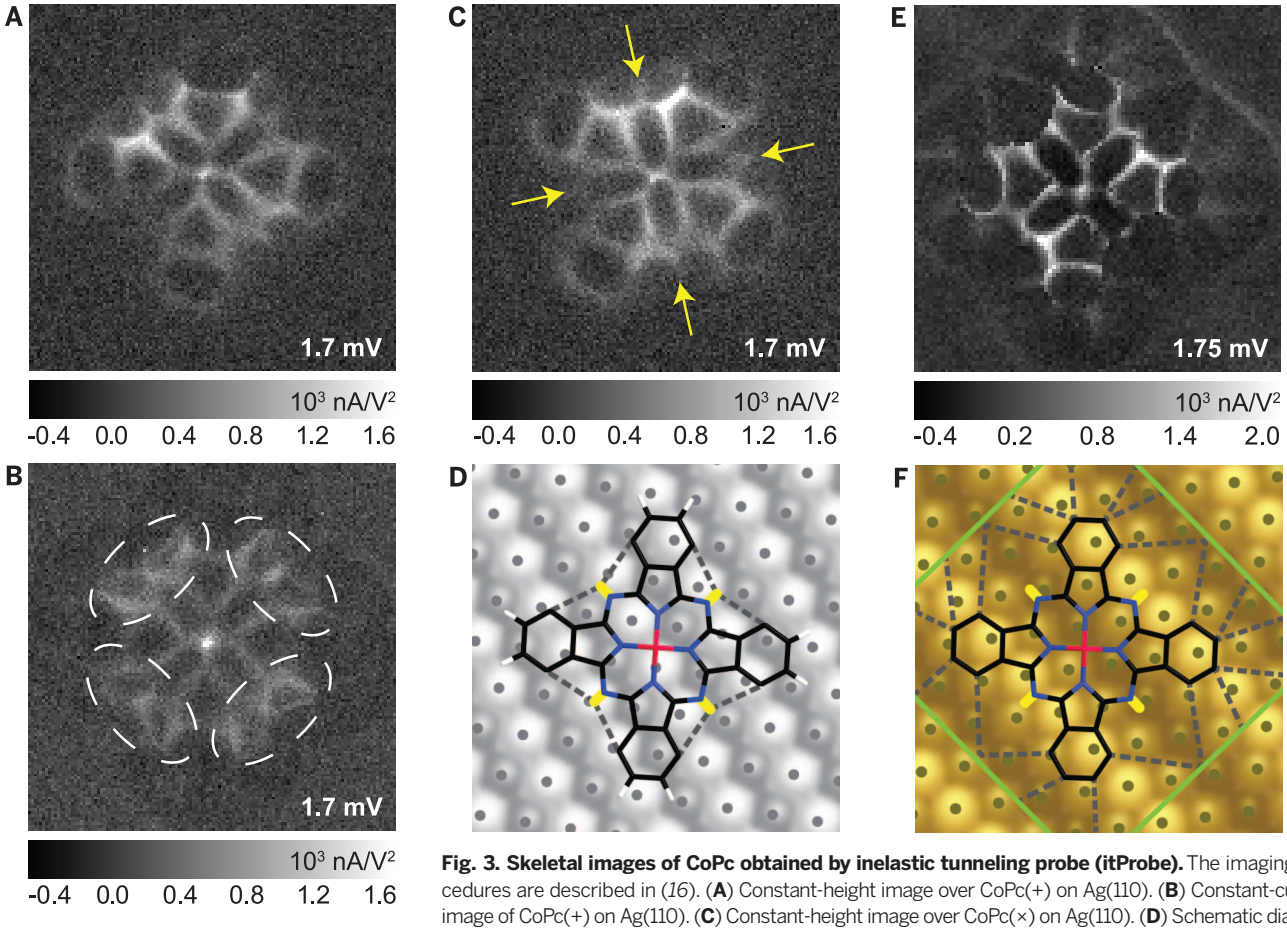

Fig. 3. Skeletal images of CoPc obtained by inelastic tunneling probe (itProbe). The imaging procedures are described in (*16*). (**A**) Constant-height image over CoPc(+) on Ag(110). (**B**) Constant-current image of CoPc(+) on Ag(110). (**C**) Constant-height image over CoPc(×) on Ag(110). (**D**) Schematic diagram showing the skeletal structure of CoPc(+) and the intramolecular hydrogen bonds highlighted in dashed ellipses in (B). The underlying Ag(110) surface and the adsorption geometry of CoPc(+) are determined from atomically resolved topographic images taken with a CO-terminated tip and with each CO bonded on top of an Ag surface atom. Area in (A) to (C) is 128 × 128 pixels and 20.2 Å × 20.2 Å. (**E**) Constant-current image over CoPc(+) on Au(110)2×1 surface (96 × 96 pixels and 21.2 Å × 21.2 Å). A rectangular boundary is resolved and is attributed to the range of electronic influence of adsorbed CoPc. A similar boundary is present on the Ag(110) surface but is less prominent than that on the Au(110) surface. (**F**) Schematic diagram showing skeletal structure of CoPc(+) on Au(110)2×1 surface. The missing surface atom rows are along the dark rows. The Co atom is over the missing row but is displaced to one side. The depicted adsorption geometry is obtained from an atomically resolved topographic image obtained with a CO-terminated tip.

hydrogen bonds (*20*, *21*). This striking feature suggests that the C-H bonds can be aligned in two directions induced by interactions with the underlying Au substrate. Evidently, a hydrogen atom can be involved in a multicenter bonding. In contrast, the structural images for CoPc on Ag(110) reveal internal bonding between each of the four lone pairs of the imine nitrogen with its two nearest-neighbor C-H bonds, forming three-center two-hydrogen bonds. These intramolecular hydrogen bonds are supposedly disfavored because of the nonlinear geometry of the C-H bond and the imine nitrogen lone pair (*21*). The images show curved bonds due presumably to this nonlinear geometry.

The multicenter hydrogen bonding is also evident in intermolecular interactions. Two CoPc molecules can be found to be adjacent to each other, such as in Fig. 4A on Ag(110). The hydrogen bonding driven by the lone pair electrons of the imine nitrogen and nearby C-H bonds is imaged by itProbe in Fig. 4B. A close-up image in Fig. 4C reveals the intramolecular and intermolecular hydrogen bonds at high spatial resolution. In Fig. 4D, the interactions among the imine nitrogen and four nearby carbon atoms are mediated by four hydrogen atoms in a five-center four-hydrogen bonding. The structural images obtained by itProbe reflect the time-averaged density of the hydrogen bonds.

The structural images were obtained by scanning in the horizontal (x) and vertical (y) directions. No noticeable differences were seen (figs. S7 and S8). The CO on the tip, however, is induced to tilt as it is brought close to the surface during imaging (*22*). This tilt gives rise to a constant offset between the structural image and the topography taken with the tip farther away from the surface where the induced tilt is absent. The amount of tilt varies for different CO-terminated tips; this offset is 1.96 Å for the specific CO-terminated tip shown in fig. S9.

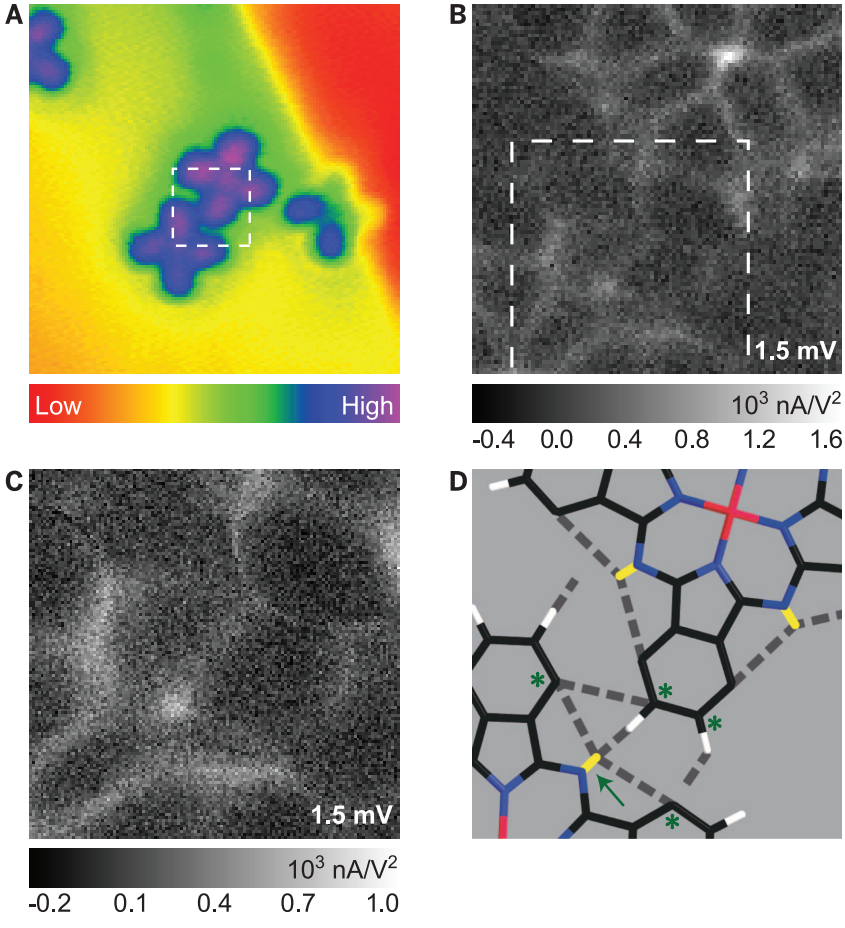

Fig. 4. Imaging the chemical bonding between a pair of CoPc on Ag(110) surface. (**A**) Constant-current topographic image (128 × 128 pixels or 60.6 Å × 60.6 Å) with sample bias V = 0.1 V and tunneling current I = 0.1 nA. (**B**) Constant-current itProbe image (100 × 100 pixels or 12.6 Å × 12.6 Å) at 1.5 mV over the white square area shown in (A). (**C**) Constant-current itProbe image (128 × 128 pixels or 8.1 Å × 8.1 Å) at 1.5 mV over the white square area shown in (B). (**D**) Schematic diagram of the image in (B), showing in dashed lines the intermolecular and intramolecular bonds involving hydrogen, and in yellow the lone pairs of imine nitrogen. Four hydrogen atoms are shared among five centers [four carbon atoms (indicated by asterisk) and one imine nitrogen (indicated by arrow)] in the five-center four-hydrogen bonds.

The contrast revealing the skeletal structure of the molecule (fig. S10) depends on the sample bias used in the imaging. The hindered translational mode of CO is low in energy (soft) and particularly sensitive to its environment, relative to the hindered rotational mode at higher energy. High-energy resolution is required for the STM to measure low-energy modes and is achieved by lowering the temperature to 600 mK (0.28 meV temperature broadening) and the modulation to 1 mV and below (*11*, *23*).

The capability of the STM to image molecular structure and chemical bonds broadens its previous applications to determine the electronic and vibrational properties of single molecules. This added capability provides much-needed knowledge to understand the relation between the structure and function of molecules. In addition to the electronic and vibrational properties, it may be possible to observe changes in geometric structure when the molecule's environment is altered by intermolecular interactions, such as in the formation of self-assembled nanostructures or in reactions on surfaces. Real-space spectroscopy and imaging by the itProbe could lead to a deeper understanding of the nature of different types of chemical bonds and related chemistry.

REFERENCES AND NOTES

1. L. Gross, F. Mohn, N. Moll, P. Liljeroth, G. Meyer, *Science* **325**, 1110–1114 (2009).
2. L. Gross *et al.*, *Science* **337**, 1326–1329 (2012).
3. D. G. de Oteyza *et al.*, *Science* **340**, 1434–1437 (2013).
4. J. Zhang *et al.*, *Science* **342**, 611–614 (2013).
5. L. Bartels *et al.*, *Phys. Rev. Lett.* **80**, 2004–2007 (1998).
6. H. J. Lee, W. Ho, *Science* **286**, 1719–1722 (1999).
7. F. J. Giessibl, *Appl. Phys. Lett.* **76**, 1470–1472 (2000).
8. J. Repp, G. Meyer, S. M. Stojković, A. Gourdon, C. Joachim, *Phys. Rev. Lett.* **94**, 026803 (2005).
9. S. W. Wu, N. Ogawa, W. Ho, *Science* **312**, 1362–1365 (2006).
10. P. Liljeroth, J. Repp, G. Meyer, *Science* **317**, 1203–1206 (2007).
11. U. Ham, W. Ho, *J. Chem. Phys.* **138**, 074703 (2013).
12. C. Weiss *et al.*, *Phys. Rev. Lett.* **105**, 086103 (2010).
13. C. Weiss, C. Wagner, R. Temirov, F. S. Tautz, *J. Am. Chem. Soc.* **132**, 11864–11865 (2010).
14. G. Kichin, C. Weiss, C. Wagner, F. S. Tautz, R. Temirov, *J. Am. Chem. Soc.* **133**, 16847–16851 (2011).
15. B. C. Stipe, M. A. Rezaei, W. Ho, *Science* **280**, 1732–1735 (1998).
16. See supplementary materials on *Science* Online.
17. W. Ho, *J. Chem. Phys.* **117**, 11033–11061 (2002).
18. J. R. Hahn, W. Ho, *Phys. Rev. Lett.* **87**, 196102 (2001).
19. L. Gross *et al.*, *Nat. Chem.* **2**, 821–825 (2010).
20. I. Rozas, I. Alkorta, J. Elguero, *J. Phys. Chem. A* **102**, 9925–9932 (1998).
21. T. Steiner, *Angew. Chem. Int. Ed.* **41**, 48–76 (2002).
22. A. J. Weymouth, T. Hofmann, F. J. Giessibl, *Science* **343**, 1120–1122 (2014).
23. L. J. Lauhon, W. Ho, *Rev. Sci. Instrum.* **72**, 216–223 (2001).

ACKNOWLEDGMENTS

Supported by the Chemical Science, Geo- and Bioscience Division, Office of Science, U.S. Department of Energy, under grant DE-FG02-04ER15595.

SUPPLEMENTARY MATERIALS

www.sciencemag.org/content/344/6186/885/suppl/DC1
Materials and Methods
Figs. S1 to S10
Reference (*24*)

14 March 2014; accepted 29 April 2014
10.1126/science.1253405

Real-space imaging of molecular structure and chemical bonding by single-molecule inelastic tunneling probe

Chi-lun Chiang, Chen Xu, Zhumin Han and W. Ho (May 22, 2014)
Science **344** (6186), 885-888. [doi: 10.1126/science.1253405]

Editor's Summary

Probing bonding profiles with a CO tip

Greater resolution has been achieved in atomic force microscopy by terminating the tip with a sharper probe: an adsorbed CO molecule. Chiang *et al.* now show that the adsorbed CO tip can reveal the bonding within cobalt phthalocyanine molecules absorbed on silver or gold surfaces. Inelastic tunneling spectroscopy reveals variations in the vibration excitation of the CO molecule that can map out the internal bonding of the molecules, as well as hydrogen bonding between molecules.

Science, this issue p. 885